Contents list available at IJRED website

International Journal of Renewable Energy Development

Journal homepage: https://ijred.undip.ac.id

Research Article

Numerical Investigation of Solidity Effect Based on Variable Diameter on Power Performance of H-type Darrieus Vertical Axis Wind Turbine (VAWT)

Muhamad Fadhli Ramlee[1], Shaikh Zishan[1], Wan Khairul Muzammil[2], Ahmad Fazlizan[1*]

[1]*Solar Energy Research Institute (SERI), Universiti Kebangsaan Malaysia, 43600 Bangi, Selangor, Malaysia*

[2]*Faculty of Engineering, Universiti Malaysia Sabah, Jalan UMS, Kota Kinabalu 88400, Malaysia*

Abstract. Renewable energy resources especially wind energy, have seen significant growth in the worldwide energy market as clean energy sources. This has brought attention to areas with low and moderate wind speeds. Small-scale Darrieus vertical axis wind turbine (VAWT) with omnidirectional capability captures potential energy in these areas at a cost-effective scale. Numerous studies have been conducted to optimise their design, hence improving the performance of these turbines. Turbine solidity, σ, representing the ratio of the overall area of the blades over the swept area of the turbine, is one of the influential geometrical factors that significantly affect wind turbine performance. Previous studies on solidity focused on the number of blades and blade length variations, while the study on turbine diameter is limited. Hence, this paper intends to numerically investigate the effect of solidity that corresponds to different turbine diameters. Power performance and flow characteristics are investigated closely according to different solidity, σ and tip speed ratios, λ using high-fidelity computational fluid dynamic (CFD) method, which solves the unsteady Reynolds-Averaged Navier-Stokes (RANS) equations. Solidity and tip speed ratios vary within a wide range of 0.3 – 0.7 and 0.5 – 4.5, respectively. The results show that decreasing the turbine solidity from 0.7 to 0.3 could significantly increase the maximum power coefficient, Cp, by 30%. However, turbine with high solidity (σ = 0.7) generate much higher instantaneous moment coefficient, Cm than the low solidity turbine (σ = 0.3), but at lower λ and a narrower range of λ. The difference in turbine's performance between high and low solidity turbine is attributed to stall experienced by the blade at low λ and the blockage effect experienced by the turbine at moderate to high λ that significantly influence the energy generation at downstream region.

Keywords: Solidity, computational fluid dynamic, H-type Darrieus, vertical axis wind turbine, wind energy

@ The author(s). Published by CBIORE. This is an open access article under the CC BY-SA license (http://creativecommons.org/licenses/by-sa/4.0/).

Received: 27th Jan 2022; Revised: 5th April 2022; Accepted: 10th April 2022; Available online: 25th April 2022

1. Introduction

Wind energy plays a significant role in developing renewable energy due to its outstanding contribution to CO_2 reduction worldwide. Wind turbines for energy generation do not release any emission that contributes to pollution. Generating energy from wind may also reduce the need for electricity from fossil fuels, reducing total CO_2 emissions. Considering the total emissions throughout the lifecycle, including the mining of raw material, manufacturing, maintenance, etc., the greenhouse gas emissions from the wind energy systems were only 124 gCO_2-eq/kWh, which is very low compared to the photovoltaic systems (300 gCO_2-eq/kWh) (Amponsah *et al.* 2014). Furthermore, the advancement of modern wind turbines has attracted much attention as green energy generators both onshore and offshore. Until now, discussions are still ongoing globally regarding the future of wind energy research and R&D directions of wind energy technology (Bianchini *et al.* 2018; Bilgili *et al.* 2021; Kamani & Kamali 2021). As more studies presently focus on wind turbines for urban applications (Chong *et al.* 2019; Chong *et al.* 2013; Fazlizan *et al.* 2019), VAWTs are receiving increasing attention in this regard, thanks to their several advantages, the primary being omnidirectional, where it can capture wind energy from every direction. In addition, previous studies also showed that VAWTs perform better in urban areas, where the wind condition is highly turbulent and unsteady compared to HAWTs. The simple structure, easy maintenance, less visual aesthetic disturbance, and low noise and vibration level make VAWTs even more attractive.

Based on the above benefits, it seems that the applications of VAWT have a promising future. Still, specific problems remain to be settled, such as optimising the VAWTs design to improve the turbine's efficiency and maximising the power output. Moreover, designing VAWT

* Corresponding author
Email: a.fazlizan@ukm.edu.my (A.Fazlizan)

https://doi.org/10.14710/ijred.2022.44431
ISSN: 2252-4940/© 2022.The Author(s). Published by CBIORE

that can generate high annual energy output at relatively low wind speed has been regarded as an alternative approach to making small-scale wind turbines suitable for the urban environment (Chen *et al.* 2015). The performance of these VAWTs needs to be analysed by predicting their characteristics and fundamental understanding of the flow field around these wind turbines (Subramanian *et al.* 2017). Thus, to benefit from the advantages of VAWTs for the aforementioned locations, their aerodynamic and power performance needs to be further improved (Rezaeiha *et al.* 2019).

Numerical methods such as computational aerodynamic model and computational fluid dynamic (CFD) are an essential step during the initial phase of the design process of VAWT, where they allow designers to test numerous turbine configurations in complex wind conditions. Moreover, they provide a first prediction of the turbine performance, which are essential for the first selection of geometrical and operational properties of the turbine. However, obtained numerical data still need to be validated against experimental data to ensure the reliability and accuracy of the simulation results (Nguyen *et al.* 2020; Vergaerde *et al.* 2019). Performing CFD calculations provides knowledge of the flow and all the necessary details, which can help better understand VAWTs at an affordable cost. For that reason, such features make CFD technology gain more attention among researchers than experimental and any other numerical methods. Few CFD studies regarding VAWT performance evaluation are already available in the literature (Arpino *et al.* 2018; Bel Mabrouk & El Hami 2019; Chen *et al.* 2017; Li *et al.* 2018; Sobhani *et al.* 2017; Wang & Zhuang 2017).

Turbine solidity is one of the essential geometrical parameters that significantly impact the power performance of VAWTs. Solidity is defined as the ratio of the area of the overall blades over the swept area of the turbine, based on Equation (1):

$$\sigma = \frac{N.c}{D} \quad (1)$$

where *N, c,* and *D* are the number of blades, blade chord length, and turbine diameter, respectively. An optimal turbine solidity would maximise the output power, where the optimum value could be dependent on the aforementioned geometrical and various operational conditions. Many numerical and experimental studies focused on the effect of solidity on the aerodynamic properties and power performance of small-scale VAWT have been recorded in the literature (Eboibi et al. 2016; Joo *et al.* 2015; Qing'an Li *et al.* 2016, 2017; Peng *et al.* 2019; Qamar & Janajreh 2017; Rezaeiha *et al.* 2018a; Sagharichi *et al.* 2018; Singh *et al.* 2015; Subramanian *et al.* 2017). Generally, there is a reasonable consensus between all these works on the solidity effect: a high solidity turbine performs well at low λ. In contrast, a low solidity turbine performs better at moderate to high λ. Previous research above shows that increasing rotor solidity could increase the rotor's starting torque and power output, optimising the turbine power performance. However, to the best of our knowledge, the existing literature has the following limitations:

- Solidity study conducted mainly focus on changing blade chord length and number of blades. Changing chord length naturally modifies blade Reynolds number; therefore, the findings in previous studies could have been influenced by the Reynolds number effect, such as the dynamic stall and flow curvature effect, which will significantly affect the turbine performance
- The number of studies on the impact of solidity at fixed R_e and turbines with different diameters is limited.

Therefore, in this paper:

- The solidity effect is studied within a wide range of solidity from a low value of 0.3 to a relatively high value of 0.7 for five-turbine configurations with different diameters, i.e., 1.0 m, 0.75 m, 0.6 m, 0.5 m and 0.43 m which will vary the solidity of σ = 0.3, 0.4, 0.5, 0.6 and 0.7, respectively.
- The evaluation is based on high-fidelity CFD technology, validated with published numerical and experimental power performance data. In total, 50 simulations were performed.
- The findings of this study are intended to provide an in-depth understanding of the impact of solidity power performance of small scale Darrieus VAWTs

Acknowledging the limitation of 2D CFD in predicting aerodynamic characteristics of a wind turbine with high accuracy, this study sufficiently provides a general understanding of the performance of 3-bladed VAWT with different solidity at different λ. It helps the reader get a general idea about the coefficient of moment, Cm and coefficient of power, Cp, and flow events/phenomena that could affect the turbine's performance at specific operational conditions.

2. Materials and Methods

2.1. Geometrical and operational parameters of the turbine

A 3-bladed H-type Darrieus VAWT equipped with a symmetric NACA0018 airfoil section is used, as depicted in Fig. 1. The geometrical and operational parameters of the turbine are tabulated in Table 1. The rotor solidity, σ, is calculated using Equation (1), while the tip speed ratio, λ, can be calculated using Equation (2) as expressed below:

$$\lambda = \frac{\omega . R}{U} \quad (2)$$

where ω is the rotor rotational speed in rad/s, R is the rotor diameter, and U is the free-stream wind speed.

The usual practice in the literature is to increase or decrease the number of blades or blade chord length to alter the solidity, but in the present approach, the rotor diameter was varied to alter the same. Table 2 shows the five configurations of the turbine with a range of rotor diameter (D) from 0.43 m to 1 m that were employed to study the flow field and aerodynamic forces acting on the blades. The number of blades, *N* and chord length, *c* is kept constant at 3 and 0.1 m.

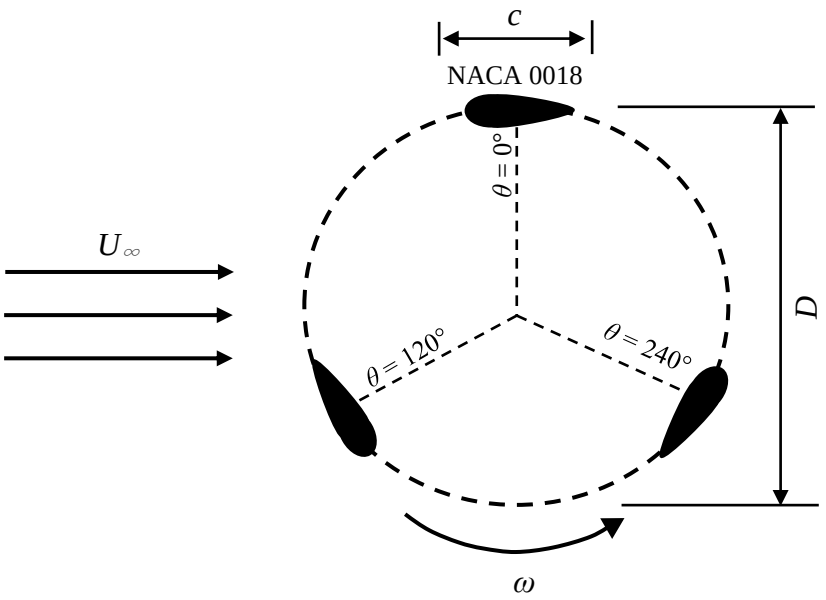

Fig 1. Schematic of the turbine

Table 1
Geometrical and operational parameters of the turbine

Parameter	Value	Parameter	Value
Number of blades, N	3	Solidity	0.3 -0.7
Diameter, D [m]	0.43 - 1	Tip speed ratio	0.5 - 4.5
Airfoil	NACA0018	Freestream velocity, U_∞ [m/s]	8.0
Airfoil chord, c [m]	0.1	Rotational speed [rad/s]	72.0

Table 2
Different geometrical configurations of the turbine

Solidity	No. of blades	Chord lengths (m)	Diameter (m)
0.3	3	0.1	1.00
0.4	3	0.1	0.75
0.5	3	0.1	0.60
0.6	3	0.1	0.50
0.7	3	0.1	0.43

2.2. CFD simulation strategy

Presently, VAWT performance evaluation using the CFD approach received much attention due to the advancement of computational technology. Table 3 summarises the CFD simulation on VAWTs configurations by the previous studies. The comparison shows the consensus on several computational settings, including the boundary conditions at the inlet, outlet and domain wall, the size of the computational domain, the algorithm for the pressure-velocity coupling, etc. In these studies (Arab *et al.* 2017; Meana-Fernández *et al.* 2018; Onol & Yesilyurt 2017), 2D CFD analysis has been performed as an alternative to the experimental approach to study the flow properties and aerodynamic performance of VAWT. Based on these studies, it has been proven that a 2D CFD model is sufficient in predicting VAWT's aerodynamic and power performance. The influence of 3D effects such as blade tip effects and the presence of central shaft and supporting arms are neglected but deemed acceptable since these effects are considered secondary (Danao *et al.* 2014). Therefore, a 2D CFD model has been employed in this study.

An extensive comparative analysis conducted by Rezaeiha (Rezaeiha et al. 2019) on seven commonly-used turbulence models for CFD simulations of VAWTs shows that Shear Stress Transport (SST) model variants, i.e. SST *k-ω*, SST *k-ω* with additional intermittency (SSTI) and transition SST (TSST), are capable in accurately

predicting the details of the VAWT's performance and exhibit reasonable agreement with the experimental results. Moreover, transitional SST *k-ω* versions (SSTI and TSST) are highly recommended, especially in the transitional flow regime. Therefore, in all simulations, the 4-equation transition SST is chosen as the turbulence model. The model is an improvement over the previous 2-equation SST *k-ω* turbulence model, where it solves two additional equations for intermittency γ and momentum-thickness Reynolds number(Langtry *et al.* 2006; Menter *et al.* 2005). Apart from the sensitivity study mentioned earlier, CFD analysis using transition SST has proven successful by (Bangga 2019; Chen *et al.* 2017; Daróczy *et al.* 2018; Mantravadi et al. 2019; Rocha *et al.* 2016), which further provides confidence for the application of this turbulence model.

The numerical calculation of the flow for the entire domain is governed by the unsteady, incompressible Navier-Stokes equations using the commercial package ANSYS FLUENT CFD software. This code uses the finite volume method to solve the governing equations. A pressure-based solver was selected following the Semi-Implicit Method for Pressure Linked Equations (SIMPLE) scheme for pressure-velocity coupling. The SIMPLE algorithm provides sufficient accuracy with reasonable computational cost and time compared to the Semi-Implicit Method for Pressure Linked Equations-Consistent (SIMPLEC) algorithm. In addition, the Pressure Implicit with Splitting of Operator (PISO) algorithm is commonly used to solve transient problems with a large time-step (C. Li et al. 2018). Considering the flow in this study that requires a small time-step, the SIMPLE algorithm is selected with second-order implicit transient formulation for improved accuracy. Second-order schemes are used for both temporal and spatial discretisation.

Angular time-step plays a vital role in the accuracy of the simulation results, and employing a suitable time-step is crucial. From the literature, it was proven that the time-step corresponding to the rotation of 1° and above is insufficient in providing a precise solution, especially at low tip speed ratios. Therefore, the time-step of 0.1° is selected for all simulations in this study. To achieve a consistent variation of instantaneous moment coefficient, C_m production throughout the entire rotation, the simulation was set to run for 21 revolutions due to the unsteadiness in the C_m variation during the initial revolutions. Further details about the angular time-step and the number of revolutions for convergence can be found in the literature (Rezaeiha et al. 2018b). The simulation is considered to have converged when it reaches a consistent/steady-state while achieving low residuals ($<1x10^{-5}$) for a complete revolution. Twenty iterations were set for each time-step to make the solution converge at each physical time-step. The evaluated C_m for the three blades were monitored and recorded to calculate the averaged power coefficient, C_p of the VAWT using Equation (3).

$$C_p = C_m.\lambda \tag{3}$$

2.3. Computational domain and grid

A suitable computational domain and mesh sizing are the critical steps in correctly reproducing high-accuracy fluid-dynamic phenomena (Lanzafame et al. 2013). In this paper, the computational domain has been divided into three sub-domains: the outer stationary domain, the inner rotational domain and the control circle domains, surrounded by the rotational domain. The computational domains are extended sufficiently to avoid blockage effects and flow disturbances that might affect the simulation results. The sensitivity study conducted by (Rezaeiha et al. 2018b) provides an extensive guideline for 2D CFD analysis. The distance of the inlet and outlet from the centre of the turbine is set at 15D and 10D (D; turbine diameter). The upper and lower sides of the domain are extended by 10D in each direction from the rotating centre of the turbine, and the rotating domain is set to 1.5D. The computational domains and mesh configuration schematic are shown in Fig. 2 and 3, respectively. The boundary conditions of the domain are inlet velocity of 8 m/s, pressure outlet of 0 Pa and symmetry wall at both sides of the domain. No-slip boundary conditions on the blade wall are specified.

Table 3
Different geometrical configurations of the turbine

Author	A. Rezaeiha (Rezaeiha *et al.* 2017a)	Z. Wang (Wang & Zhuang 2017)	E. Sobhani (Sobhani *et al.* 2017)	J. Chen (J. Chen *et al.* 2015)
Geometrical and operational parameters				
Model	2D	3D	2D	2D
Airfoil	NACA0015	NACA0018	NACA 0012	NACA0015
Chord length	0.0575 m	0.12 m	0.086 m	0.25 m
Computational domain and settings				
Mesh type	structured	structured	unstructured	unstructured
Domain size	30D*20D	-	-	20D*10D
Turbulence model	Transition SST	RE k-ε	SST k-ω	SST k-ω
Y^+	≤ 1	30 - 50	~ 2.9	1-1.7
Algorithm	SIMPLE	SIMPLE	PISO	SIMPLE
Scheme	2nd order	2nd order	2nd order	2nd order
Boundary conditions				
Inlet	Velocity-inlet	Velocity-inlet	Velocity-inlet	Velocity-inlet
Outlet	Pressure-outlet	Pressure-outlet	Pressure-outlet	Pressure-outlet
Wall	Symmetry, no-slip	Symmetry, no-slip	Symmetry, no-slip	Symmetry, no-slip

2.4. Grid Independency

A grid refinement study has been carried out using three different computational grid sizes, as listed in Table 4, to ensure the independency of the numerical results from grid mesh resolution. The azimuthal increment used in this grid refinement study is 0.5° with 21 revolutions for each grid configuration. Fig. 4 shows the plot of the C_m for a single blade during the last revolution versus the azimuthal angle. As presented in the figure, the differences between C_m of the medium and fine grids are insignificant than those between coarse and fine grids. A notable difference in C_m can be observed when the grid is refined from coarse to medium, where the coarse grid tends to over-predict the C_m at the upstream region ($45° < \theta < 135°$). Based on this grid refinement analysis, the medium size of grid resolution results is found to produce sufficiently accurate results with reasonable cost and time required for the calculation. Therefore, the medium grid with 443,628 cells is used for the rest of the following numerical simulation in this paper.

2.5 Model validation

To ensure the accuracy of the simulation results, a set of validation studies is performed which employed the same computational settings used as described in Sections 2.2 and 2.3. The study investigates an H-type Darrieus VAWT with three symmetric blades NACA0021. The turbine has a diameter of 1 m ($\sigma = 0.25$) and operates at a range of tip speed ratio ($1.43 \leq \lambda \leq 3.29$) with an incoming free stream of 9 m/s. While the geometrical and operational parameters were changed according to the selected reference case, the computational domains, grid, settings and boundary conditions remain the same. The validation study compares the calculated turbine C_p against the CFD study by Rezaeiha et al. (Rezaeiha et al. 2017b) and experimental data by Castelli et al. (Raciti Castelli et al. 2011). The comparison of the calculated C_p was made at a range of λ, as shown in Fig. 5.

A good agreement is observed between the present CFD results and published data from the figure. The present CFD can replicate the trend of change in C_p produced by the experimental data relatively well, with minor quantitative differences observed at certain λ. Moreover, the present CFD shows better agreement with experimental data than the CFD study by Castelli et al. (Raciti Castelli et al. 2011). This can be attributed to the fact that the present study strongly follows the computational setting guidelines by Rezaeiha et al. in choosing the optimum turbulence model, computational domain size and settings for an accurate 2D CFD simulation. The good consensus between experimental data, the CFD study by Rezaeiha et al. and this present study further increase the confidence in the reliability of the present CFD results.

Overall, the present CFD tends to over-predict the C_p, especially at moderate to high λ. The figure shows that the present CFD results started to deviate at $\lambda = 3.0$. The prediction C_p of simulation is 33% higher than the experimental data, and the deviation continues as λ increases. This might be the result of the inability of 2D CFD simulation to consider blade tip losses and other 3D effects in the calculation. Another possible reason is the absence of connecting arms or struts in a simplified 2D CFD modelling that might contribute to the overestimation of 2D CFD simulation. Based on the aforementioned comparison and discussion for the validation study, the present CFD results are believed to provide an accurate and reliable prediction of experimental data.

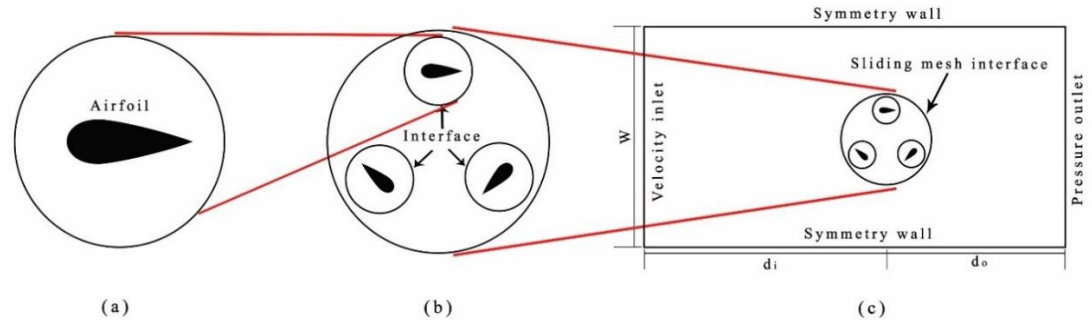

Fig 2. Schematic of the computational domain: d_i and d_o, distance from the turbine centre to the inlet and outlet; d_c, the diameter of the rotating core; W, the width of the domain.

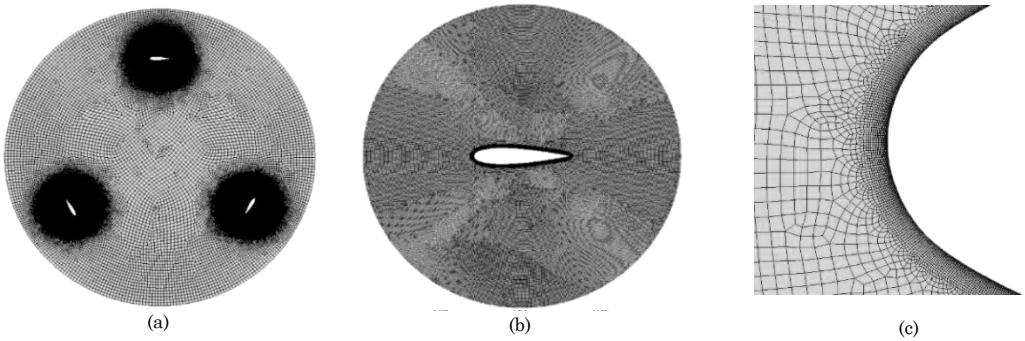

Fig 3. Mesh settings and size (non-scaled): (**a**) rotating sub-domain; (**b**) control circle, and (**c**) boundary layers near the blade.

Table 4
Details of the computational grids used.

Grid size	Coarse	Medium	Fine
No. of cells	283762	443628	649796

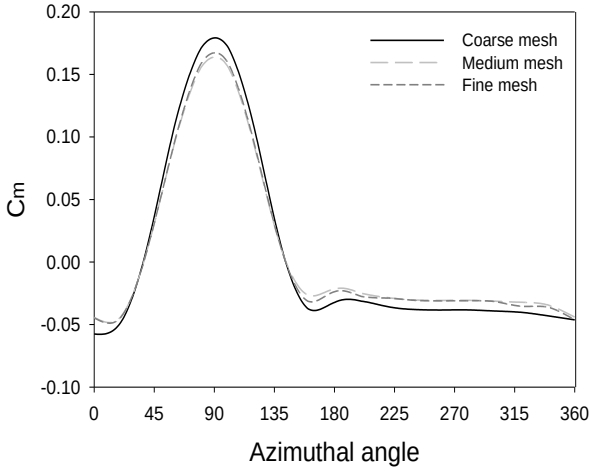

Fig 4. The plot of C_m-θ for a single blade during the last revolution for three different grid sizes

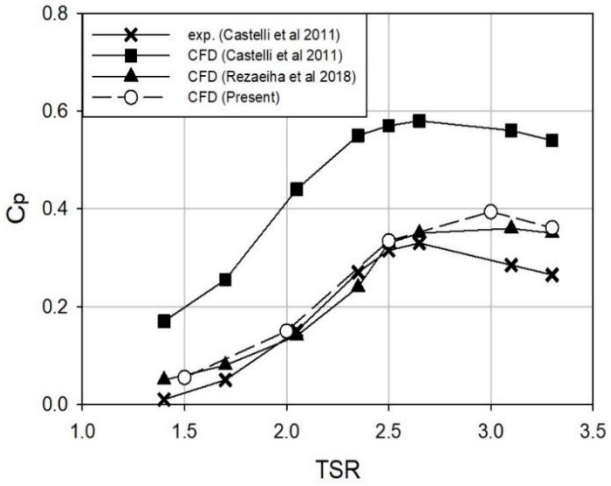

Fig 5. Comparison of C_p against numerical and experimental data by Rezaeiha et al. (Rezaeiha et al. 2017b) and Castelli et al. (Raciti Castelli et al. 2011)

3. Results and Discussion

3.1 Effect of solidity on the performance of VAWT at various TSR

To investigate the effect of solidity, the rotor diameter is taken as a variable parameter while the number of blades and the chord length are kept constant. Despite having a simple design structure, H-Darrieus VAWT has highly complicated aerodynamic characteristics due to the relative flow velocities and a large variation of the angle of attack during each revolution.

Fig. 6(a-b) shows the performance variation for 3-bladed VAWT with a wide range of solidity from 0.3 to 0.7. In this study, the H-Darrieus used shows a similar performance trend of increased power coefficient, C_p, with the tip speed ratio, λ. As shown in Fig. 6(a), the value of C_p increases with the increase of λ for all turbine configurations and drops after achieving the maximum value. When the solidities of the turbine are σ = 0.3, 0.4, 0.5, 0.6 and 0.7, the maximum C_p are about C_p = 0.402, 0.397, 0.362, 0.302 and 0.280, respectively. However, increasing the solidity from 0.3 to 0.7 decreases the maximum C_p by 30% and shifts the peak curves to the left. A low solidity turbine performs better at moderately high λ. In contrast, a high solidity turbine works optimally at relatively low λ. For instance, turbine with σ = 0.3 achieves maximum C_p at λ = 3.0 while turbine with σ = 0.7 achieves maximum C_p at λ = 1.5. The figure also indicates that the change in solidity influence the operating range of the turbine, where the low solidity turbine has a wider operating range of λ as compared to the high solidity turbine that starts to produce net negative C_m at λ ≥ 3.0..

Fig. 6(b) shows the C_m-λ curves according to solidity. As shown in the figure, a remarkable increase of the C_m with the increase of solidity appears in the area of low λ (λ < 2). A high solidity rotor (σ = 0.7) reaches maximum C_m faster than a medium and low solidity turbine. Singh et al. (Singh et al. 2015) mentioned that a high torque production in the low λ range is vital to overcome the starting load in the initial operation, hence improving the self-starting capability of a straight-bladed VAWT. Therefore, as shown in the figure, the enhancement of the C_m production by a high solidity rotor in low λ could be recommended to overcome the self-starting problem of an H-type Darrieus VAWT.

The optimal performance of the VAWT can be seen more clearly from the contours of C_p illustrated in λ – σ space in Fig. 7. The contour highlights the optimal parameters concerning the solidity and tip speed ratio. It also illustrates the regions of poor turbine performance which need to be avoided when designing VAWT. Red spots imply the optimal condition for the turbine with the highest performance. In contrast, blue spots indicate regions with poor performance, i.e., a high solidity turbine at high λ or a low solidity turbine at low λ. As presented by these figures (Fig. 6(a-b) and Fig. 7), the optimal performance of the turbine is obtained either at a combination of low σ and high λ or vice versa. This means that, at a given wind speed, when the turbine is rotating faster (higher ω), the optimal performance is achieved with a bigger diameter (lower σ), while if the turbine is rotating slower (lower ω), the optimal performance is obtained for a smaller diameter (higher σ).

Tip speed ratio, λ, is one of the critical operational parameters as it determines the variation range of angle of attack, α, on the blades during each rotation. Finding the optimum tip speed ratio, $\lambda_{opt,}$ is crucial in optimising the power output of a VAWT. Low λ corresponds to large α, which will lead to significant flow separation on blades and power loss if the stall angle is exceeded. Meanwhile, high λ corresponds to small α, which could mean that the turbine generates less power than its actual capability.

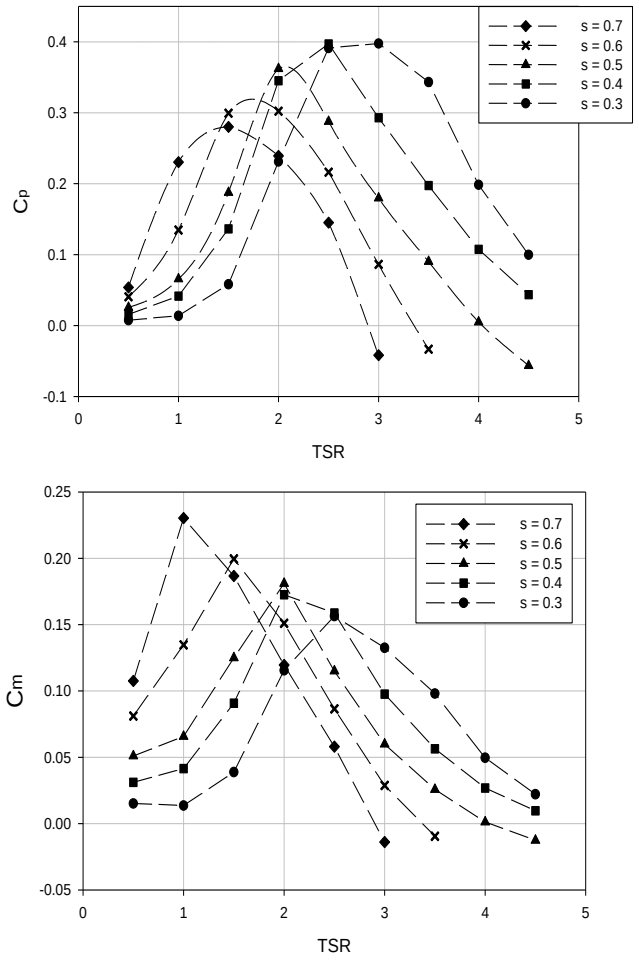

Fig 6. Performance of the turbine according to σ and λ (a) power coefficient, C_p; (b) instantaneous moment coefficient, C_m

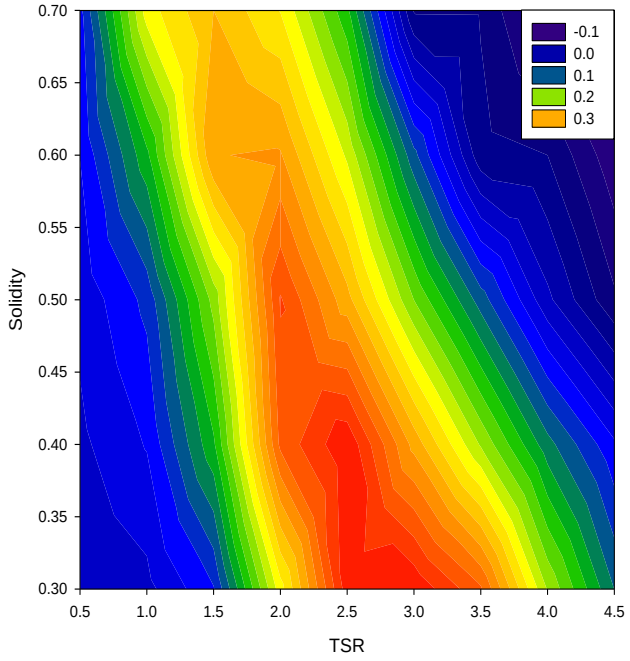

Fig 7. The contour of Cp according to σ and λ

Fig. 8 shows the power coefficient against solidity for constant λ. It can be seen from the figure that the optimal solidity, where the turbine achieves maximum C_p, decreases as the λ increase. For instance, the optimal solidity for turbine constantly operating at λ = 1.5 is σ = 0.6. Meanwhile, the optimal solidity decreases to σ = 0.5 and σ = 0.4 when the turbine operated at λ = 2.0 and λ = 2.5, respectively. Moreover, the figure also indicates that the changes in solidity at low λ (λ ≤ 0.5) has an insignificant influence on the turbine performance, whereas increasing solidity from 0.3 to 0.7 at λ = 0.5 only increase the C_p from 0.008 to 0.054. Significant changes in C_p can only be seen at λ ≥ 1.0.

3.2 Moment coefficient

Fig.9(a-b) shows the comparison of the total instantaneous moment coefficient, C_m, for the three turbine configurations at two different λ to illuminate the behaviour of the turbine with different solidity at low λ (λ = 1.0) and mid-high λ (λ = 2.5). Three peaks can be observed from the figures during each rotation as in this study; the wind turbine has three rotating blades. Therefore, the first blade is placed at θ = 0°, the second blade is at θ = 240°, and the third is at θ = 120°. When the blades are at an azimuthal angle of θ = 0° or θ = 180°, the magnitude of drag force is large since the wind direction is parallel to the drag vector; thus, the lift produced at this point is minimum. As a result, the torque in this region is negative, and the blade passes through this area with inertia.

As observed in Fig. 9(a), at λ = 1.0, a low solidity turbine (larger diameter) experiences unstable during the revolution and early drop after reaching the peak. Besides, it produces a significant negative torque, especially at 90° ≤ θ ≤ 135°, which indicates its practicality in producing a consistent positive torque. During the revolution, the turbine with medium and smaller diameter experiences a steadier sinusoidal behaviour. The rotor with the medium solidity (σ = 0.5) fluctuates between negative and positive torque while its averaging produces a positive net torque. Meanwhile, a high solidity turbine (σ = 0.7) displays much higher C_m than the other two lower solidity turbines and is able to maintain positive C_m throughout the entire rotation. This behaviour marks the turbine's ability with a smaller diameter (high σ) in producing the largest amount of energy at low λ compared to the medium and larger rotor diameter.

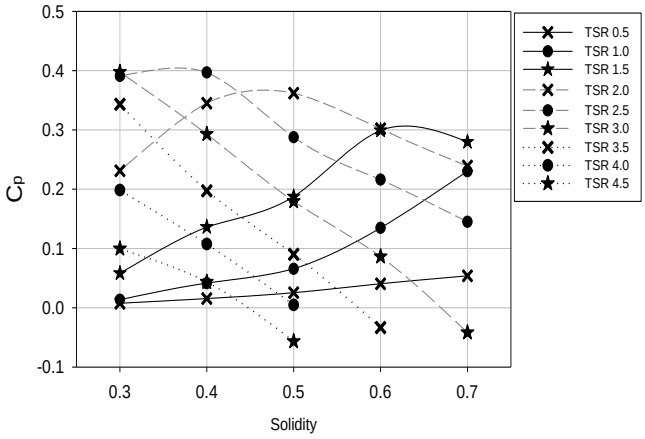

Fig 8. Power coefficient against the solidity

Meanwhile, the evaluated C_m for the three configurations at $\lambda = 2.5$ can be seen in Fig. 9(b). In contrast to the turbine's behaviour at low λ, all three configurations experience stable sinusoidal oscillatory behaviour. However, the low solidity rotor shows better performance with steadier behaviour and higher torque production than at low λ resulting in the best performance among the three configurations. The VAWT, at a solidity of 0.3, manages to maintain a positive torque throughout the entire revolution, signalling its capability in producing net positive torque at high λ.

Generally, the torque produced by the turbine during revolution depends highly on the magnitude of lift force acting on the blades. At low λ, the velocity of the incoming flow is almost similar to the tangential velocity of the rotating blade. Therefore, the angle of attack is large and could exceed the stall angle. For instance, at $\lambda = 1.0$ (Fig. 9(a)), the C_m of $\sigma = 0.3$ suddenly decrease after reaching maximum at $\theta \approx 80°$. This indicates that the blade experiences a dynamic stall due to the large angle of attack, leading to a significant reduction of lift force acting on the blade. As a result, the C_m behaviour becomes asymmetric and unsteady.

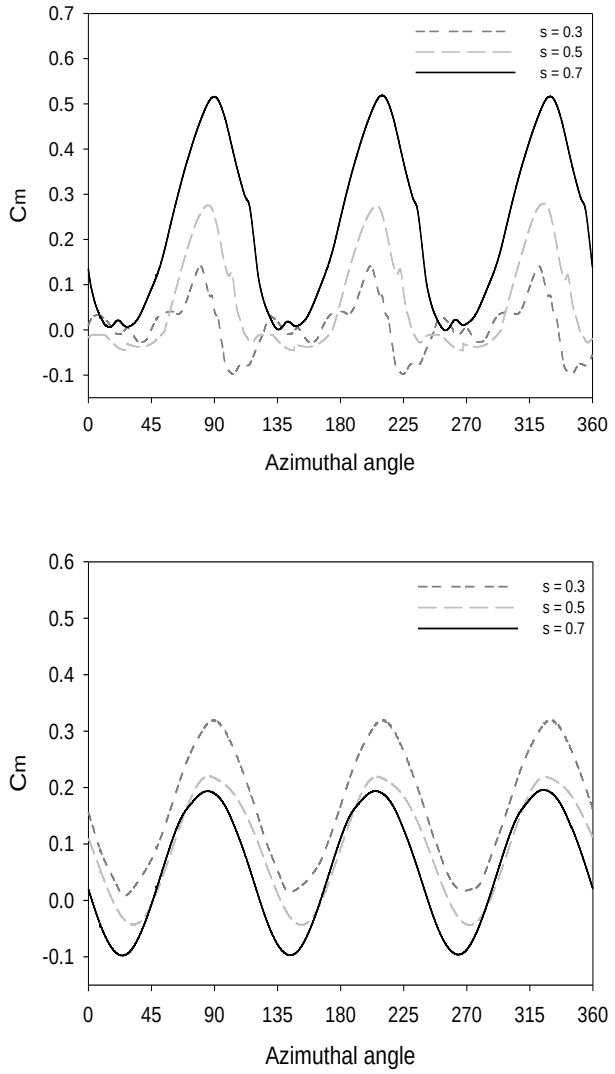

Fig 9. Instantaneous moment coefficient, C_m variations for different solidities; (a) $\sigma = 0.3, 0.5, 0.7$ at $\lambda = 1.0$, (b) $\sigma = 0.3, 0.5, 0.7$ at $\lambda = 2.5$

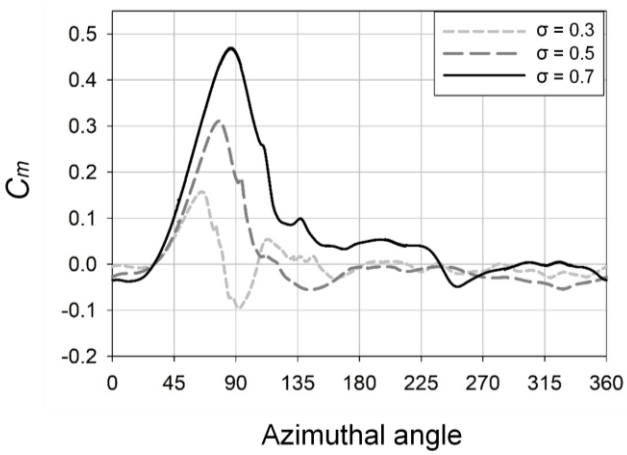

Fig 10. Moment coefficient against azimuthal angle for the turbine solidity of 0.3, 0.5 and 0.7 at $\lambda = 1.0$

3.3 Velocity contour

Fig. 10 depicts the Cm-θ curve on a single blade, while the plot contours of velocity with streamlines in the vicinity of the blade at $50° \leq \theta \leq 130°$ are shown in Fig. 11. Both results are taken at the last turbine revolution at $\lambda = 1.0$. The contours highlight the flow characteristics and aerodynamic properties for high solidity turbine ($\sigma = 0.7$) and low solidity turbine ($\sigma = 0.3$) at low λ ($\lambda = 1.0$). Following observations can be made from the figures:

1. The early drop in C_m that occur on the blade has been delayed to later θ as σ increase. For instance, the C_m of $\sigma = 0.3$ suddenly drop at $\theta = 50°$ instead of $\theta = 90°$ for $\sigma = 0.5$ and 0.7. This is thought to result from the higher rotational velocity for high solidity turbine due to a smaller diameter for the same λ, resulting in delays in the flow separation and dynamic stall on the blade. In the case of $\sigma = 0.3$, the low rotational velocity increases the angle of attack. As a result, the blade experiences a stall where the C_m suddenly drop early ($\theta < 90°$). However, for turbine $\sigma = 0.7$, the low angle of attack due to higher rotational velocity does not exceed the stall angle. Hence, the C_m is smooth and decreases gradually at $\theta \approx 90°$, producing the highest C_m. The observed trend of early drop in C_m at low λ is also in agreement with the studies on solidity effects (Wang & Zhuang 2017).
2. Apart from the drop in C_m, the dynamic stall experienced by the blade could also be reflected by the formation of a laminar separation bubble (LSB) that occurs earlier for low solidity turbines. Moreover, increasing σ could not only delay the formation of LSB but also could (i) delay the bursting of LSB and follow-up deep-stall, (ii) reduce the trailing-edge vortices, and (iii) delays the trailing-edge separation. A similar event could also be found in a study of the solidity effect by Rezaeiha et al. (Rezaeiha et al. 2018a). Moreover, this contour has revealed that increasing σ, especially at low λ, substantially influences the flow separation dynamic stall on the blade.
3. To further understand the effect of flow separation and dynamic stall phenomena on the performance of VAWT, Bangga et al. [30,31] conducted a series of CFD simulations to study complex aerodynamic

characteristics due to flow separation and dynamic stall onset. The study involves a detailed analysis of wake characteristics and the development of shedding vortices around the rotor.

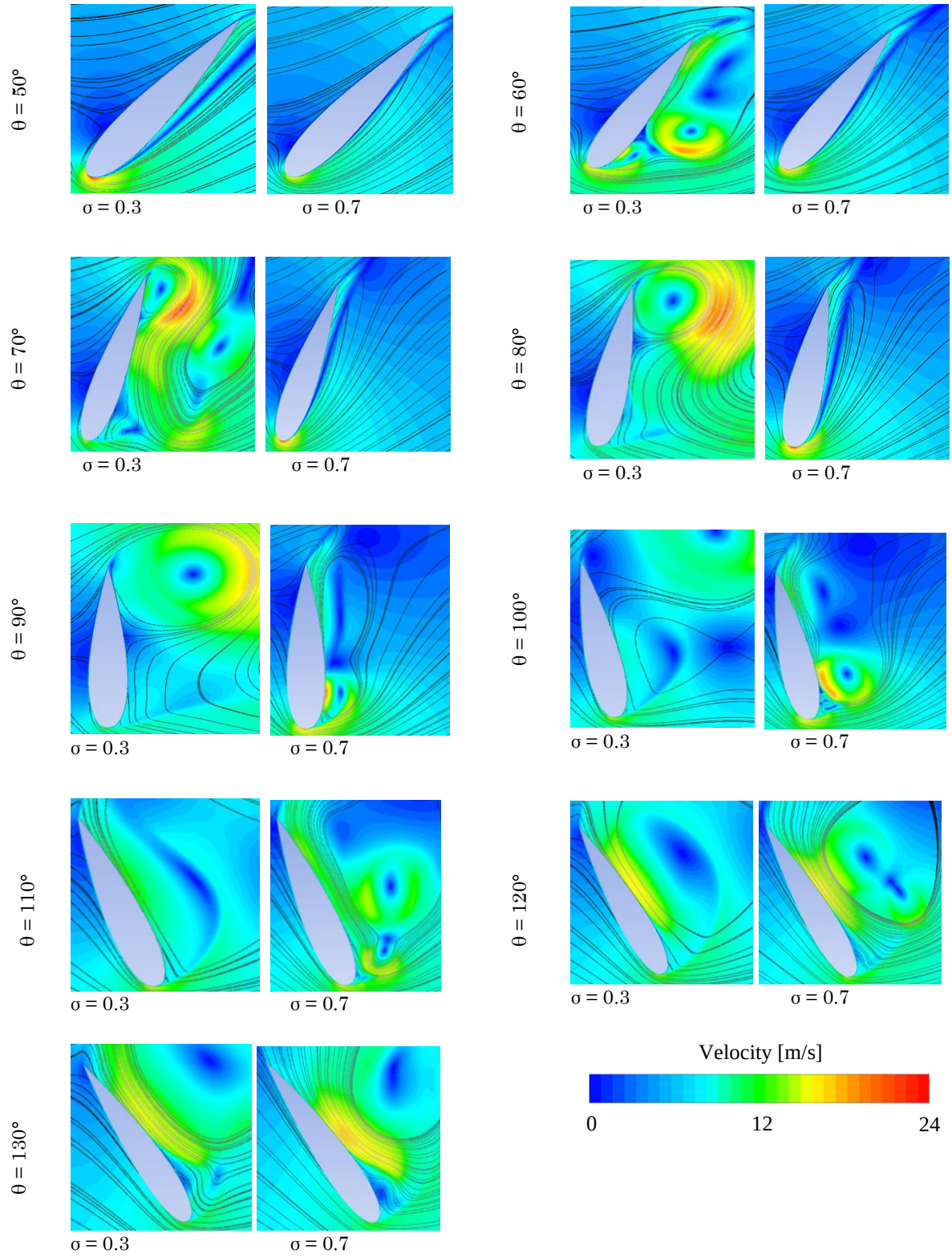

Fig 11. Velocity contour plots with streamlines for σ = 0.3 and 0.7 at λ = 1.0 and azimuth angle from 50° to 130

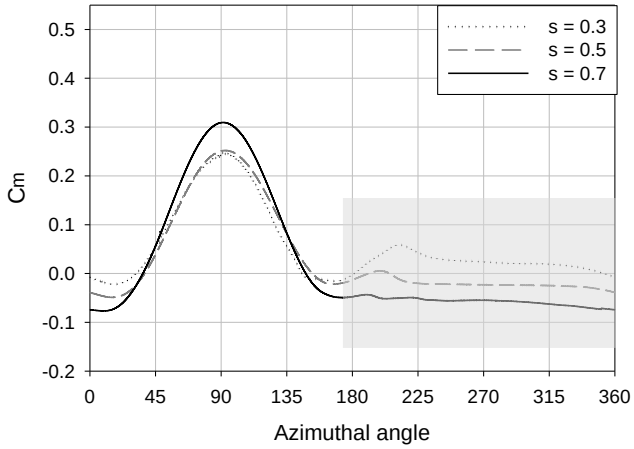

Fig 12. Velocity contour plots for σ = 0.3, 0.5 and 0.7 at λ = 2.5.

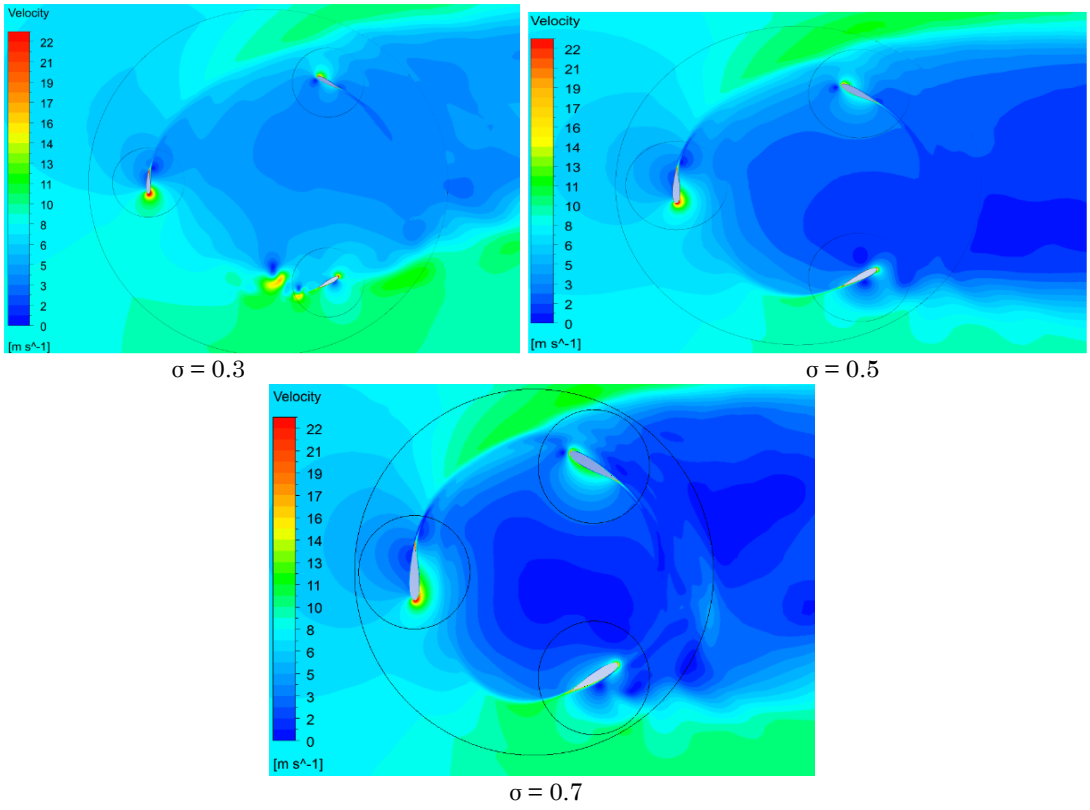

Fig 13. Velocity contour plots for σ = 0.3, 0.5 and 0.7 at λ = 2.5.

Figures 12 and 13 show the Cm-θ curve on a single blade and the velocity contour plots for three turbine configurations of different diameters at λ = 2.5, respectively. As observed from these plots, changes in turbine diameter induce a significant solidity effect that dramatically influences the performance of the VAWT. As the solidity increases by decreasing the turbine diameter, the low-velocity region at downstream becomes more intense as the high solidity turbine obstructs much of the incoming stream. The higher solidity turbine continues to impede the incoming flow. It vigorously disperses the fluid onto the sides, diverting the flow into a higher and favourable pressure gradient at both sides of the turbine. The obstructed flow has also enlarged the turbine's upstream induction field, which could lead to the formation of a pressure gradient in the region at $45° \leq \theta \leq 135°$, thus affecting the power extraction by the blade.

The higher side velocity also contributed to earlier instability of the separating shear layer leading to a faster vortex formation, as apparent in the high solidity turbine's velocity contours. This high attained side velocity could weaken the rotor performance. A high

solidity turbine has a pronounced interaction between blade and formation of shedding vortices. On the other hand, the low solidity turbine has less obstruction of the free-stream than the high solidity turbine; hence, the blades in the downstream region can extract energy from the incoming wind throughout the rotation. This could improve the overall performance of the turbine. Therefore, at moderate to high λ, the low solidity turbine is preferable in the power performance demonstrated by its ability to produce net positive C_m.

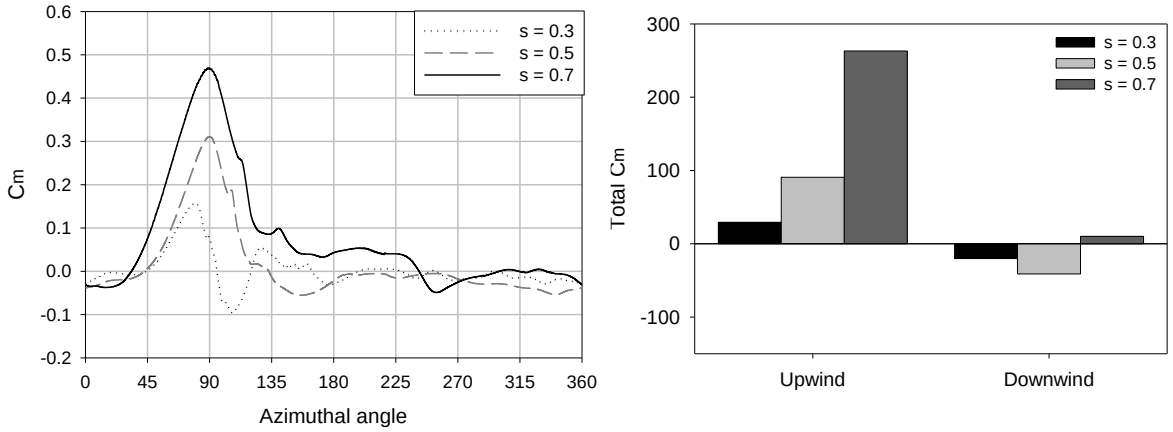

(a) λ = 1.0

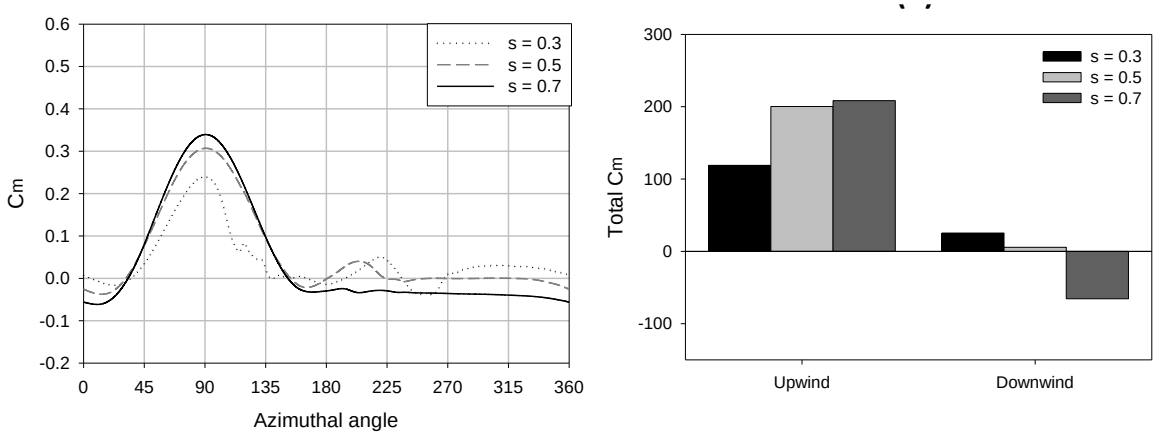

(b) λ = 2.0

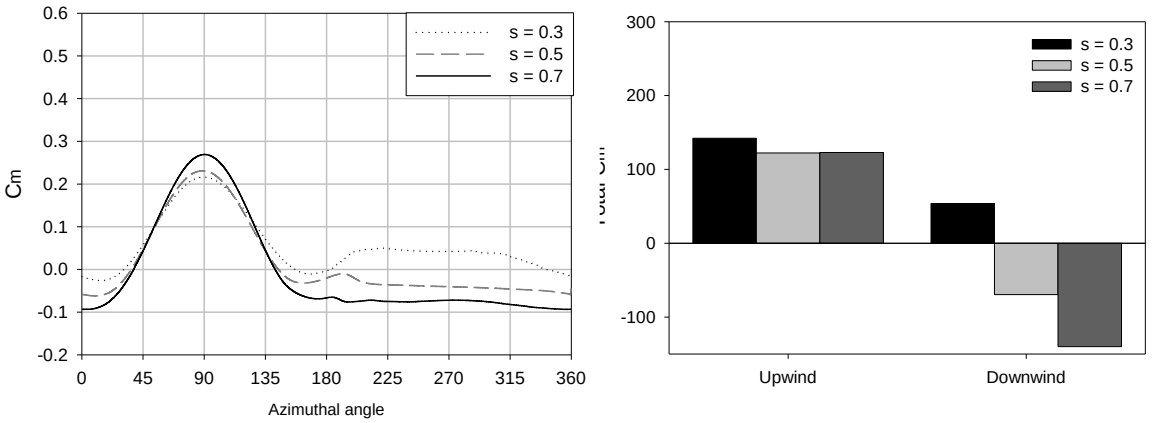

(c) λ = 3.0

Fig 14. Instantaneous moment coefficient, C_m plot and contribution during the last turbine revolution for σ = 0.3, 0.5 and 0.7 at λ = 1.0, 2.0 and 3.0

3.4 Contribution by region

The instantaneous moment coefficient, $C_{m,}$ during the last turbine revolution for three turbine solidities, σ = 0.3, 0.5 and 0.7 at three different tip speed ratios, λ = 1.0, 2.0 and 3.0, are compared in Fig. 14(a-c). From these figures, the following observations can be made:

1. At λ = 1.0 (Fig. 14(a)), increasing σ from 0.3 to 0.7 increases the total C_m in the upstream region. This is reflected by the total C_m of the turbine at σ = 0.7 is the highest among the three configurations. Moreover, only turbine σ = 0.7 is capable of generating positive $C_{m,}$ although the amount is insignificant, while σ = 0.3 and 0.5 produce negative $C_{m,}$ indicating the impracticality of both turbines in low λ.
2. At λ = 2.0 (Fig. 14(b)), there is an increase in total C_m by turbine σ = 0.3 and 0.5 at the upstream. Similarly, at downstream, both turbines can generate positive C_m in contrast to that in λ = 1.0, although the total C_m produced is relatively small. On the other hand, turbine σ = 0.7 began to decline in performance with a decrease in upstream C_m production. In addition, the turbine also produces a considerably high amount of negative C_m at downstream, which could affect the total production of C_m by the turbine
3. At λ = 3.0 (Fig. 14(c)), all three turbines produce an almost similar amount of total C_m at upstream. However, there is a significant difference in total C_m between each turbine, where turbine σ = 0.5 and 0.7 produced a remarkable amount of negative C_m, with the highest negative C_m generated by σ = 0.7. In contrast, the positive C_m yield by turbine σ = 0.3 increases, contributing to the net positive C_m produced by the turbine.

The analysis reveals that the upwind region of VAWT becomes the most important region where it contributes the most to the total power production. On the other hand, only a low solidity turbine can generate positive Cm in the downwind region. This analysis shows that one of the strategies to enhance the power production of a VAWT is to look at the local power production where the negative C_m should be minimised.

4. Conclusion

Solidity is one of the key geometrical parameters that hugely influence turbine performance. Therefore, the focus of this paper is to numerically investigate the effect of solidity on the power performance and flow characteristics of a 3-bladed H-type Darrieus VAWT using high fidelity unsteady CFD simulation method to provide a better understanding and to help designers.

In this study, a series of 2D CFD simulation has been performed on a 3-bladed Darrieus VAWT according to various solidities ($0.3 < \sigma < 0.7$) and tip speed ratios solidities ($0.5 < \lambda < 4.5$). The numerical calculation utilises the ANSYS Fluent CFD software to solve the unsteady Reynolds-Averaged Navier-Stokes (RANS) equations with the 4-equation transition Shear-Stress Transport (SST) as the turbulence model. To assess the accuracy of the simulation results, the present data were compared to the published data. An excellent agreement is obtained as the present CFD can replicate the changing trend in Cp produced by the experimental data relatively well with minor quantitative differences at certain λ.

The simulation results show that the flow characteristics of the VAWT are significantly influenced by the changes in solidity at different λ. The performance of the turbines is attributed to two primary effects observed in this study: the flow separation on the blade at low λ and the blockage effect at high λ. The relative velocity and angle of attack with respect to the rotating blade change significantly due to the effects. The changes greatly affect the power performance of each turbine configuration with different solidity at different λ. The low solidity turbine experiences stalls at low λ due to lower rotational velocity as the turbine diameter is bigger, while the high solidity turbine has the highest performance. The occurrence of flow separation near the blade wall at λ = 1.0 (low λ) is reflected by the formation of a laminar separation bubble (LSB) that forms earlier for low solidity turbine (σ = 0.3) and contributes to the early drop in Cm at θ ~ 50° instead of θ ~ 90° for the medium at high solidity turbine (σ = 0.5 and 0.7).

In contrast, as the λ increases, the performance of the high solidity turbine begins to decrease as the turbine experiences a significant blockage effect and higher blade-wake-interactions, while the low solidity turbine performs better at this point. It was shown that at λ = 2.5, a remarkable flow obstruction occurs for a high solidity turbine (σ = 0.7) where a near-zero flow velocity region is formed downstream, indicating its impracticality to produce net positive torque at moderate-high λ.

However, the evaluations in this study are only made based on 2D CFD simulation, where 3D effects such as blade tip vortex and the influence of shaft and supporting arms are not taken into consideration. Therefore, in our future work, fully resolved 3D CFD simulation and wind tunnel experiments should be performed to improve the accuracy of the results, especially in predicting the tip loss effects at high λ and dynamic stall at low λ that are not sufficiently captured in the present work, hence, providing an in-depth understanding of the performance of VAWT..

Acknowledgements

The research is funded by the Ministry of Higher Education of Malaysia under the Fundamental Research Grant Scheme (FRGS/1/2019/TK03/UKM/02/6).

References

Amponsah, N. Y., Troldborg, M., Kington, B., Aalders, I. & Hough, R. L. (2014). Greenhouse gas emissions from renewable energy sources: A review of lifecycle considerations. *Renewable and Sustainable Energy Reviews* 39461–475; doi:https://doi.org/10.1016/j.rser.2014.07.087

Arab, A., Javadi, M., Anbarsooz, M. & Moghiman, M. (2017). A numerical study on the aerodynamic performance and the self-starting characteristics of a Darrieus wind turbine considering its moment of inertia. *Renewable Energy* 107298–311; doi:10.1016/j.renene.2017.02.013

Arpino, F., Scungio, M. & Cortellessa, G. (2018). Numerical performance assessment of an innovative Darrieus-style vertical axis wind turbine with auxiliary straight blades.

Energy Conversion and Management 171769–777; doi:https://doi.org/10.1016/j.enconman.2018.06.028

Bangga, G. (2019). Numerical studies on dynamic stall characteristics of a wind turbine airfoil. *Journal of Mechanical Science and Technology* 33(3), 1257–1262; doi:10.1007/s12206-019-0225-1

Bel Mabrouk, I. & El Hami, A. (2019). Effect of number of blades on the dynamic behavior of a Darrieus turbine geared transmission system. *Mechanical Systems and Signal Processing* 121562–578; doi:https://doi.org/10.1016/j.ymssp.2018.11.048

Bianchini, A., Balduzzi, F., Ferrara, G., Persico, G., Dossena, V. & Ferrari, L. (2018). A Critical Analysis on Low-Order Simulation Models for Darrieus Vawts: How Much Do They Pertain to the Real Flow? *Journal of Engineering for Gas Turbines and Power* 141(1), doi:10.1115/1.4040851

Bilgili, M., Tumse, S., Tontu, M. & Sahin, B. (2021). Effect of Growth in Turbine Size on Rotor Aerodynamic Performance of Modern Commercial Large-Scale Wind Turbines. *Arabian Journal for Science and Engineering* 46(8), 7185–7195; doi:10.1007/s13369-021-05364-6

Chen, J., Yang, H., Yang, M. & Xu, H. (2015). The effect of the opening ratio and location on the performance of a novel vertical axis Darrieus turbine. *Energy* 89819–834; doi:10.1016/j.energy.2015.05.136

Chen, W.-H., Chen, C.-Y., Huang, C.-Y. & Hwang, C.-J. (2017). Power output analysis and optimisation of two straight-bladed vertical-axis wind turbines. *Applied Energy* 185223–232; doi:https://doi.org/10.1016/j.apenergy.2016.10.076

Chong, W.-T., Muzammil, W. K., Ong, H.-C., Sopian, K., Gwani, M., Fazlizan, A. & Poh, S.-C. (2019). Performance analysis of the deflector integrated cross axis wind turbine. *Renewable Energy* 138675–690; Retrieved from https://www.sciencedirect.com/science/article/pii/S0960148119301491?dgcid=author

Chong, W. T., Poh, S. C., Fazlizan, A., Yip, S. Y., Koay, M. H. & Hew, W. P. (2013). Exhaust air energy recovery system for electrical power generation in future green cities. *International Journal of Precision Engineering and Manufacturing* doi:10.1007/s12541-013-0138-3

Danao, L. A., Edwards, J., Eboibi, O. & Howell, R. (2014). A numerical investigation into the influence of unsteady wind on the performance and aerodynamics of a vertical axis wind turbine. *Applied Energy* 116111–124; doi:10.1016/j.apenergy.2013.11.045

Daróczy, L., Janiga, G. & Thévenin, D. (2018). Computational fluid dynamics based shape optimisation of airfoil geometry for an H-rotor using a genetic algorithm. *Engineering Optimization* 50(9), 1483–1499; doi:10.1080/0305215X.2017.1409350

Eboibi, O., Danao, L. A. M. & Howell, R. J. (2016). Experimental investigation of the influence of solidity on the performance and flow field aerodynamics of vertical axis wind turbines at low Reynolds numbers. *Renewable Energy* 92474–483; doi:https://doi.org/10.1016/j.renene.2016.02.028

Fazlizan, A., Muzammil, W. K., Ismail, M. A., Ramlee, M. F. & Ibrahim, A. (2019). Skewed wind flows energy exploitation in built environment. *Alam Cipta* 12(SI 1), 53–60; Retrieved from https://www.scopus.com/inward/record.uri?eid=2-s2.0-85073147419&partnerID=40&md5=4c2cc37b8d023eaf50ccca66bdf8cea5

Joo, S., Choi, H. & Lee, J. (2015). Aerodynamic characteristics of two-bladed H-Darrieus at various solidities and rotating speeds. *Energy* 90439–451; doi:10.1016/j.energy.2015.07.051

Kamani, O. & Kamali, R. (2021). Performance and Aeroacoustic Noise Prediction for an Array of Small-Scale Vertical Axis Wind Turbines. *Iranian Journal of Science and Technology - Transactions of Mechanical Engineering* 45(1), doi:10.1007/s40997-020-00385-2

Langtry, R. B., Menter, F. R., Likki, S. R., Suzen, Y. B., Huang, P. G. & Volker, S. (2006). A Correlation-Based Transition Model Using Local Variables---Part II: Test Cases and Industrial Applications. *Journal of Turbomachinery* 128(3), 423–434;

Lanzafame, R., Mauro, S. & Messina, M. (2013). Wind turbine CFD modeling using a correlation-based transitional model. *Renewable Energy* 5231–39; doi:10.1016/j.renene.2012.10.007

Li, C., Xiao, Y., Xu, Y. lin, Peng, Y. xin, Hu, G. & Zhu, S. (2018). Optimisation of blade pitch in H-rotor vertical axis wind turbines through computational fluid dynamics simulations. *Applied Energy* 2121107–1125; doi:10.1016/j.apenergy.2017.12.035

Li, Qing'an, Maeda, T., Kamada, Y., Murata, J., Shimizu, K., Ogasawara, T., Nakai, A., et al. (2016). Effect of solidity on aerodynamic forces around straight-bladed vertical axis wind turbine by wind tunnel experiments (depending on number of blades). *Renewable Energy* 96928–939; doi:https://doi.org/10.1016/j.renene.2016.05.054

Li, Qing'an, Maeda, T., Kamada, Y., Shimizu, K., Ogasawara, T., Nakai, A. & Kasuya, T. (2017). Effect of rotor aspect ratio and solidity on a straight-bladed vertical axis wind turbine in three-dimensional analysis by the panel method. *Energy* 1211–9; doi:https://doi.org/10.1016/j.energy.2016.12.112

Mantravadi, B., D., U., Sriram, K., Mohammad, A., Vaitla, L. & Velamati, R. K. (2019). Effect of solidity and airfoil on the performance of vertical axis wind turbine under fluctuating wind conditions. *International Journal of Green Energy* 16(14), 1329–1342; doi:10.1080/15435075.2019.1671408

Meana-Fernández, A., Solís-Gallego, I., Fernández Oro, J. M., Argüelles Díaz, K. M. & Velarde-Suárez, S. (2018). Parametrical evaluation of the aerodynamic performance of vertical axis wind turbines for the proposal of optimized designs. *Energy* 147504–517; doi:10.1016/j.energy.2018.01.062

Menter, F. R., Langtry, R., Völker, S. & Huang, P. G. (2005). Transition Modelling for General Purpose CFD Codes. *Engineering Turbulence Modelling and Experiments 6* 31–48; doi:10.1016/B978-008044544-1/50003-0

Nguyen, M. T., Balduzzi, F., Bianchini, A., Ferrara, G. & Goude, A. (2020). Evaluation of the unsteady aerodynamic forces acting on a vertical-axis turbine by means of numerical simulations and open site experiments. *Journal of Wind Engineering and Industrial Aerodynamics* 198104093; doi:https://doi.org/10.1016/j.jweia.2020.104093

Onol, A. O. & Yesilyurt, S. (2017). Effects of wind gusts on a vertical axis wind turbine with high solidity. *Journal of Wind Engineering and Industrial Aerodynamics* 162(June 2016), 1–11; doi:10.1016/j.jweia.2017.01.003

Peng, Y.-X., Xu, Y.-L., Zhan, S. & Shum, K.-M. (2019). High-solidity straight-bladed vertical axis wind turbine: Aerodynamic force measurements. *Journal of Wind Engineering and Industrial Aerodynamics* 18434–48; doi:https://doi.org/10.1016/j.jweia.2018.11.005

Qamar, S. B. & Janajreh, I. (2017). A comprehensive analysis of solidity for cambered darrieus VAWTs. *International Journal of Hydrogen Energy* 42(30), 19420–19431; doi:https://doi.org/10.1016/j.ijhydene.2017.06.041

Raciti Castelli, M., Englaro, A., Benini, E., Castelli, M. R., Englaro, A. & Benini, E. (2011). The Darrieus wind turbine: Proposal for a new performance prediction model based on CFD. *Energy* 36(8), 4919–4934; doi:10.1016/j.energy.2011.05.036

Rezaeiha, A., Kalkman, I. & Blocken, B. (2017)a. CFD simulation of a vertical axis wind turbine operating at a moderate tip speed ratio: Guidelines for minimum domain size and azimuthal increment. *Renewable Energy* 107373–385; doi:10.1016/j.renene.2017.02.006

Rezaeiha, A., Kalkman, I. & Blocken, B. (2017)b. Effect of pitch angle on power performance and aerodynamics of a vertical axis wind turbine. *Applied Energy* 197132–150; doi:10.1016/j.apenergy.2017.03.128

Rezaeiha, A., Montazeri, H. & Blocken, B. (2018)a. Towards optimal aerodynamic design of vertical axis wind turbines:

Impact of solidity and number of blades. *Energy* 1651129–1148; doi:https://doi.org/10.1016/j.energy.2018.09.192

Rezaeiha, A., Montazeri, H. & Blocken, B. (2018)b. Towards accurate CFD simulations of vertical axis wind turbines at different tip speed ratios and solidities: Guidelines for azimuthal increment, domain size and convergence. *Energy Conversion and Management* 156301–316; doi:10.1016/j.enconman.2017.11.026

Rezaeiha, A., Montazeri, H. & Blocken, B. (2019). On the accuracy of turbulence models for CFD simulations of vertical axis wind turbines. *Energy* 180838–857; doi:10.1016/j.energy.2019.05.053

Rocha, P. A. C., Rocha, H. H. B., Carneiro, F. O. M., da Silva, M. E. V. & de Andrade, C. F. (2016). A case study on the calibration of the k–ω SST (shear stress transport) turbulence model for small scale wind turbines designed with cambered and symmetrical airfoils. *Energy* 97144–150; doi:https://doi.org/10.1016/j.energy.2015.12.081

Sagharichi, A., Zamani, M. & Ghasemi, A. (2018). Effect of solidity on the performance of variable-pitch vertical axis wind turbine. *Energy* 161753–775; doi:https://doi.org/10.1016/j.energy.2018.07.160

Singh, M. A., Biswas, A. & Misra, R. D. (2015). Investigation of self-starting and high rotor solidity on the performance of a three S1210 blade H-type Darrieus rotor. *Renewable Energy* 76381–387; doi:10.1016/j.renene.2014.11.027

Sobhani, E., Ghaffari, M. & Maghrebi, M. J. (2017). Numerical investigation of dimple effects on darrieus vertical axis wind turbine. *Energy* 133231–241; doi:10.1016/j.energy.2017.05.105

Subramanian, A., Yogesh, S. A., Sivanandan, H., Giri, A., Vasudevan, M., Mugundhan, V. & Velamati, R. K. (2017). Effect of airfoil and solidity on performance of small scale vertical axis wind turbine using three dimensional CFD model. *Energy* 133179–190; doi:https://doi.org/10.1016/j.energy.2017.05.118

Vergaerde, A., De Troyer, T., Carbó Molina, A., Standaert, L. & Runacres, M. C. (2019). Design, manufacturing and validation of a vertical-axis wind turbine setup for wind tunnel tests. *Journal of Wind Engineering and Industrial Aerodynamics* 193103949; doi:https://doi.org/10.1016/j.jweia.2019.103949

Wang, Z. & Zhuang, M. (2017). Leading-edge serrations for performance improvement on a vertical-axis wind turbine at low tip-speed-ratios. *Applied Energy* 2081184–1197; doi:10.1016/j.apenergy.2017.09.034

.

© 2022. This article is an open access article distributed under the terms and conditions of the Creative Commons Attribution-ShareAlike 4.0 (CC BY-SA) International License (http://creativecommons.org/licenses/by-sa/4.0/)